Electronic Supplementary Information (ESI)

Pore Engineering of Graphene Aerogels for Vanadium Redox Flow Batteries

Yang Yang [a,b,c,§], Wenji Ma [b], Tong Zhang [a,c], Dingding Ye [a,c], Rong Chen [a,c], Xun Zhu [a,c]

[a] Ministry of Education Key Laboratory of Low-grade Energy Utilization Technologies and Systems (Chongqing University), Chongqing 400030, China

[b] Research & Development Institute of Northwestern Polytechnical University in Shenzhen, School of Mechanical Engineering, Shenzhen 518057, China

[c] Institute of Engineering Thermophysics, Chongqing University, Chongqing 400030, China

§ Yang Yang, Ph.D., Corresponding author

E-mail: yang_yang@nwpu.edu.cn

Address: Institute of Engineering Thermophysics, Chongqing University, Chongqing 400030, China

Tel/Tax: +86-23-6510-2474

Materials and Method

System

As showed in Figure S8, the reactant solutions containing VO_2^+/VO^{2+} and V^{3+} were obtained *via* the electrolysis of 1.5 M $VOSO_4$ in 2 M H_2SO_4 in a standard electrolytic cell.[S1] The external current was fixed on 40 mA cm^{-2}. To fabricate the reactor, the positive (*i.e.* Pt plate) and negative electrode (*i.e.* PEGA) were separated by a proton exchange membrane (PEM, Nafion 117) in two chambers, as showed in Figure S9. 1.5 M $VOSO_4$ diluted in 2 M H_2SO_4 has been typically chosen as the fuel/electrolyte by previous reports. The active vanadium concentration in sulfuric-acid-based VRB is typically lower than 1.7 M due to the poor solubility and stability under high vanadium ion concentration.

Physical characterization

The surface morphology, microstructure and crystal phase composition were characterized by scanning electron microscopy equipped with energy disperse spectroscopy (SEM-EDS, VEGA 3LMU, TESCAN), transmission electron microscope (TEM, JEOL2010, Japan) and X-ray diffraction (XRD, Brucker D8, Germany). X-ray diffraction (XRD, Brucker D8, Germany) was carried out using Cu radiation with a 2θ-angle range of 15^o~60^o and a step size of 0.02^o. The Raman spectra were collected with Raman spectrometer (Reinshaw Raman, 633 nm). The average pore diameter and pore distribution were calculated from adsorption branch by Barett-Joyner-Halenda (BJH)

model, and the Brunauer-Emmett-Teller (BET) specific surface area and pore characteristics were determined from the N_2 adsorption-desorption measurement data over the relative pressure (P/P_0) (ASAP 2460, Micromeritics Inc., GA). The micropore surface area, rather than the number of micropore, was evaluated from *t-plot* theory rather than BJH adsorption model. The BJH model was not suitable for analysing the small pores (<10 nm) especially for micropores (<2 nm), because the strong interaction between the neighbouring micropore-wall made the Kelvin equation not suitable anymore.

Electrochemical characterization

Cyclic voltammetry (CV) and electrochemical impedance spectroscopy (EIS) measurements were conducted using a CHI 660E electrochemical workstation (CH Instruments Inc.). A three-electrode system was used, where PEGAs that served as the working electrode (WE), commercial platinum foam and Ag/AgCl [sat. KCl solution, +0.197 V *vs*. standard hydrogen electrode (SHE)] as the counter electrode (CE) and reference electrode (RE), respectively. The measurement was carried out in the aqueous solution of 1.5 M $VOSO_4$/2 M H_2SO_4. CV was scanned from 0.2 V to 2.1 V at the scan rate of 10 mV s^{-1}. The complete one-cycle charging-discharging property was characterized at a constant current density of 25 mA cm^{-2} by setting the voltage upper limit (charging) and voltage lower limit (discharging). [S2, S3] The variation of OCP (*vs*. time) was obtained under the low state of charge (*i.e.* 10% of state of charge). EIS test

was performed from 1 Hz to 100 kHz at 0 V. The energy efficiency (*EE*) could be calculated as the following equation (*Eq*. S1):

$$EE(\%) = \frac{discharge\ energy}{charge\ energy} \times 100\% = \frac{\int V_d I_d dt}{\int V_c I_c dt} \times 100\%$$

S1

Where V_d is the discharging voltage, V_c charging voltage, I_d discharging current, I_c charging current and t indicates corresponding time. The specific capacity (C) was calculated using the following equation (*Eq*. S2):

$$C = {}^{I_d \cdot t}\!/_{w} \qquad S2$$

Where w is the electrode weight.

Supplementary Figures and Tables

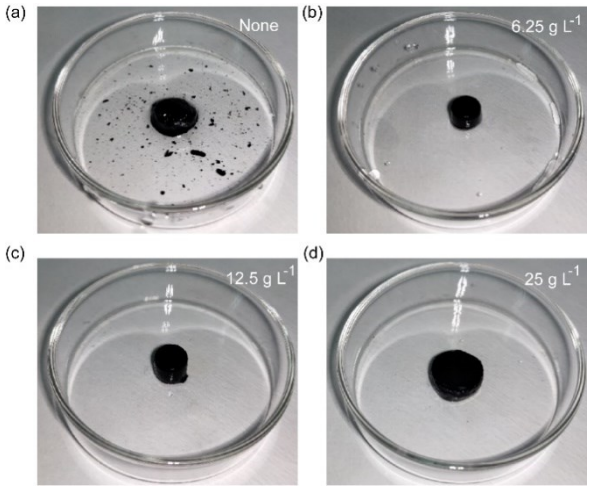

Fig. S1. (a-d) Optical images of GA, PEGA-6.25, PEGA-12.5 and PEGA-25.

Fig. S2. Optical images of PEGA with the $NaNO_3$ content of 37.5 g L^{-1}.

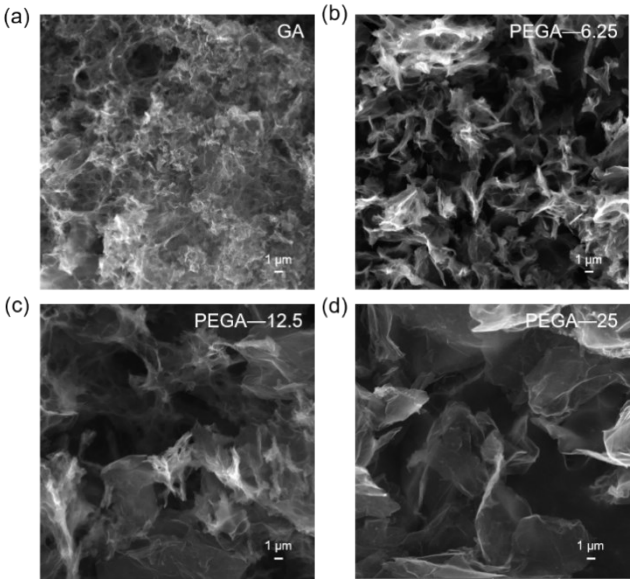

Fig. S3. Enlarged SEM images showing the porous structure of (a) GA and (b-d) PEGA with different porogen contents.

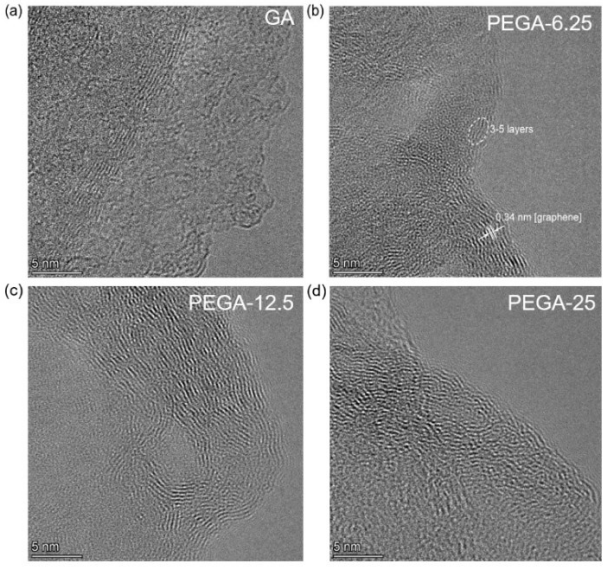

Fig.S4. TEM image showing the morphologies of (a) GA and (b-d) PEGA with different porogen contents. TEM image showing the mono-layer structure (3~5 layers) and layer space (~0.34 nm).

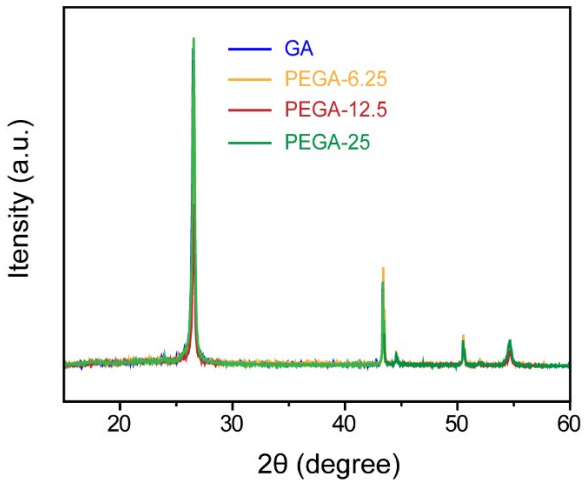

Fig.S5. XRD patterns of GA and PEGAs.

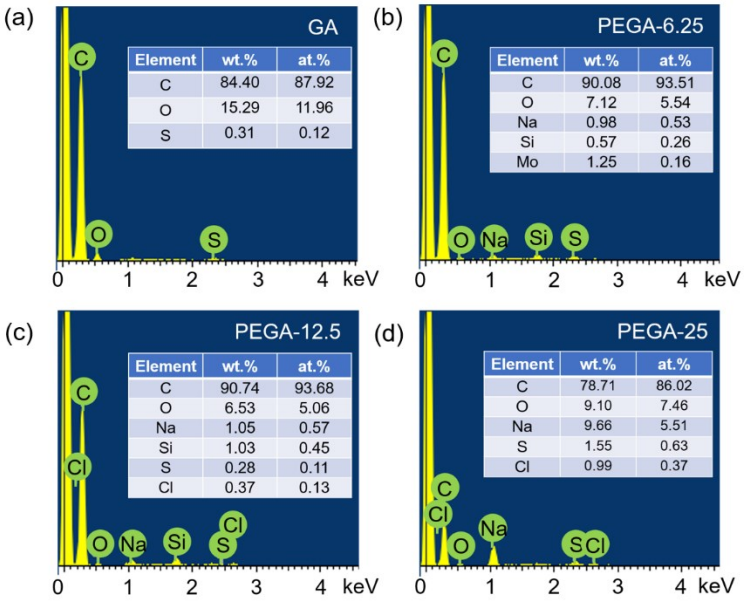

Fig.S6. EDS mapping of GA and PEGAs. Inset table summarizes the elementary contents.

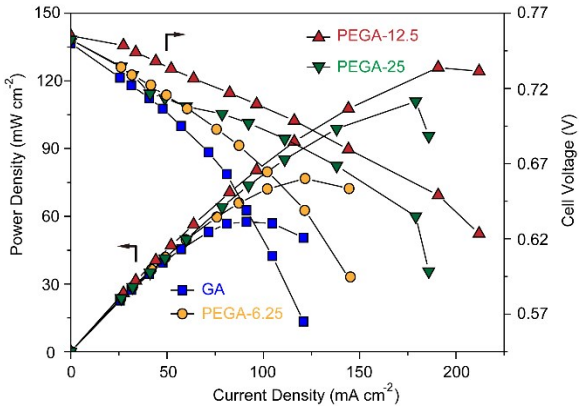

Fig. S7. Polarization and power density curves collected from VFB with GA, PEGA-6.25, PEGA-12.5 and PEGA-25.

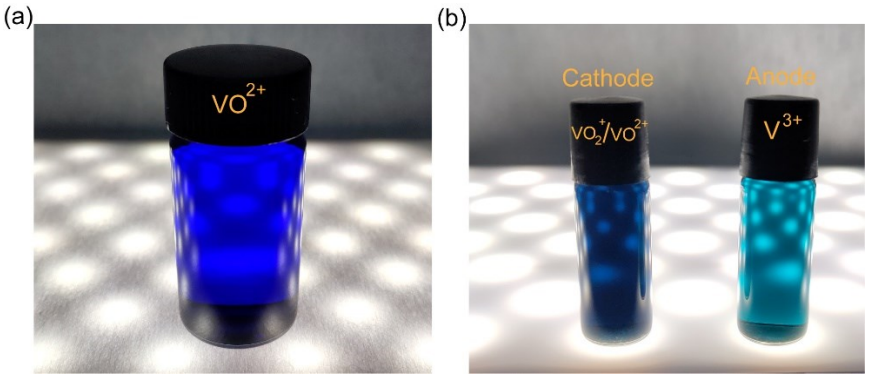

Fig.S8. Optical images of (a) VO^{2+} and (b) VO_2^+/VO^{2+} (cathode side) and V^{3+} (anode side).

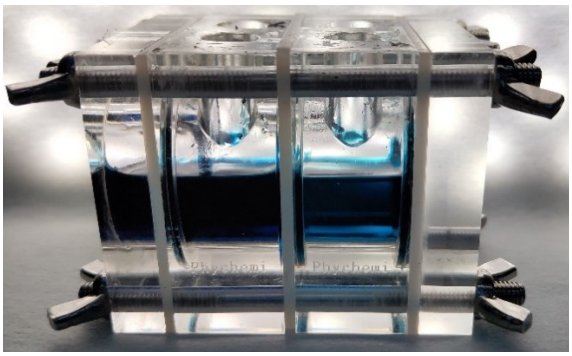

Fig.S9. Schematic illustration of VRB device with the lab-scale.

Table S1. Pore-characters of GA and PEGA with different porogen.

Property	GA	PEGA-6.25	PEGA-12.5	PEGA-25
BET surface area ($m^2\ g^{-1}$)	34.3	156.9	207.4	273.5
Average pore size (nm)	41.2	5.4	3.7	2.9
Cumulative pore volume ($cm^3\ g^{-1}$) [a]	0.046	0.13	0.09	0.082
Micropore surface area ($m^2\ g^{-1}$) [b]	64.4	67.4	148.3	122.6

Note: a. Total pore volume; b. t-plot micropore surface area.

Table S2. Parameters and performances of recently typical graphene-based electrodes in the VFB applications.

Catalyst@Electrode	**Cut-off**	**Energy Efficiency**	**Specific**	**Specific**	**Ref.**

	Potential (V)	(100%)	Capacity (Ah L^{-1})	Capacity (mAh g^{-1})	
Pore-engineered graphene aerogel	**0.3~2.2**	**85%**	**5.6**	**163.4**	**This work**
Graphene gelatum /graphite plate	0.75~1.65	82.6%	~	~	S4
Phosphonated graphene oxide	0.8~1.72	80.2%	~	~	S5
Orientated graphene oxide/Nafion	0.8~1.65	81.5-88.4%	~	~	S6
Graphene-modified carbon felt	0.8~1.6	83.3	10.9[a]	~	S7
Electro	0.7~1.72	82%	17.5[b]	116.6[b]	S8

Note: a. The value was collected at 1.6 M $V^{3.5+}$ solution; b. The value was calculated based on the electrode area (1×1 cm^2).

Supporting References

S1. W. Li, J. Liu and C. Yan, *Carbon*, 2013, **55**, 313-320.

S2. L. Yu, F. Lin, W. Xiao, L. Xu and J. Xi, *Chem. Eng. J*., 2019, **356**, 622-631.

S3. M. Jiao, T. Liu, C. Chen, M. Yue, G. Pastel, Y. Yao, H. Xie, W. Gan, A. Gong, X. Li and L. Hu, *Energy Storage Mater*., 2020, **27**, 327-332.

S4. M. Jing, C. Zhang, X. Qi, Y. Yang, J. Liu, X. Fan, C. Yan and D. Fang, *Int. J. Hydrogen Energy*, 2020, **45**, 916-923.

S5. M. Etesami, E. Abouzari-Lotf, A. Ripin, M. M. Nasef, T. M. Ting, A. Saharkhiz and A. Ahmad, *Int. J. Hydrogen Energy*, 2018, **43**, 189-197.

S6. L. Su, D. Zhang, S. Peng, X. Wu, Y. Luo and G. He, *Int. J. Hydrogen Energy*, 2017, **42**, 21806-816.

S7. D. O. Opar, R. Nankya, J. Lee and H. Jung, *Electrochim. Acta*, 2020, **330**, 135276.

S8. P. M. Nia, E. Abouzari-Lotf, P. M. Woi, Y. Alias, T. M. Ting, A. Ahmad and N. W. Che Jusoh, *Electrochim. Acta*, 2018, **297**, 31-39.

S9. M. Park, Y. Jung, J. Kim, H. Lee and J. Cho, *Nano Lett*., 2013, **13**, 4833-4839.

S10. H. Zhang, J. Wang, Q. Liu, W. He, Z. Lai, X. Zhang, M. Yu, Y. Tong and X. Lu, *Energy Storage Mater*., 2019, **21**, 154-161.

S11. M. S. Balogun, M. Yu, Y. Huang, L. Cheng, P. Fang, L. Yi, X. Lu and Y. Tong, *Nano Energy*, 2015, **11**, 348-355.

S12. A. Slesarenko, I. K. Yakuschenko, V. Ramezankhani, V. Sivasankaran, O. Romanyuk, A.V. Mumyatov, I. Zhidkov, S. Tsarev, E. Z. Kurmaev, A. F. Shestakov, O. V. Yarmolenko, K. J. Stevenson and P. A. Troshin, *J. Power Sources*, 2019, **435**, 226724.

S13. J. Cao, F. Ding, H. Chen, H. Wang, W. Wang, Z. Chen and J. Xu, *J. Power Sources*. 2019, **423**, 316-22

S14. H. Saneifar, N. Delaporte, G. Shul and D. Bélanger, *Mater. Chem. Phys*., 2019, **235**, 121739.

S15. J. Li, Z. Guo, C. Deng, Y. Gu, M. Xie, R. Xiong, Y. Xue, H. Zhao, K. Scott and X. Wu, *J. Energy Storage*, 2019, **26**, 100832.

S16. J. Lang, K. Liu, Y. Jin, Y. Long, L. Qi, H. Wu and Y. Cui, *Energy Storage Mater*., 2020, **20**, 412-416.

S17. L. Liu, L. Yang, M. Liu, X. Wang, X. Li, D. Shao, K. Luo, Z. Luo and G. Chen, *J. Energy Storage*, 2019, **25**, 100886.